Single AAV-mediated mutation replacement genome editing in limited number of photoreceptors mediate marked visual restoration

Short title: Single AAV MMEJ genome editing

Koji M Nishiguchi,[1,2†*] Kosuke Fujita,[3†] Fuyuki Miya,[4] Shota Katayama,[1] Toru Nakazawa[1,2,3*]

[1] Department of Advanced Ophthalmic Medicine, Tohoku University Graduate School of Medicine, Sendai 980-8574, Japan

[2] Department of Ophthalmology, Tohoku University Graduate School of Medicine, Sendai 980-8574, Japan

[3] Department of Ophthalmic Imaging and Information Analytics, Tohoku University Graduate School of Medicine, Sendai 980-8574, Japan

[4] Department of Medical Science Mathematics, Medical Research Institute, Tokyo Medical and Dental University, Tokyo 113-8510, Japan

[†]These authors contributed equally to the work.

[*]Corresponding authors. Tel: +81-22-717-7294

19 Koji M Nishiguchi, E-mail: nishiguchi@oph.med.tohoku.ac.jp

20 Toru Nakazawa, E-mail: ntoru@oph.med.tohoku.ac.jp

21

22 **Abstract**

23 **Supplementing wildtype copies of functionally defective genes (gene**

24 **supplementation) with adeno-associated virus (AAV) is a strategy being explored**

25 **clinically for various retinal dystrophies. However, the low cargo limit of this vector**

26 **(~5,000 bps) allows its use in only a fraction of patients with mutations in relatively**

27 **small pathogenic genes. To overcome this issue, we developed a single AAV platform**

28 **that allows local replacement of a mutated sequence with its wildtype counterpart,**

29 **based on combined CRISPR-Cas9 and micro-homology-mediated end-joining (MMEJ).**

30 **In blind mice, the mutation replacement rescued ~10% of photoreceptors, resulting in**

31 **an incredible ~10,000-fold improvement in light sensitivity and increasing visual**

32 **acuity to ~60% of the controls. Surprisingly, these effects were comparable to**

33 **restoration mediated by gene supplementation, which targets ~70% of**

34 **photoreceptors. This strategy paves the way for treatment of inherited disorders**

35 **caused by mutations in larger genes, for which conventional gene supplementation**

36 **therapy is not currently feasible.**

Introduction

Delivery of wild-type copies of the defective gene (gene supplementation) in retinal dystrophy patients with loss of function mutations via adeno-associated virus (AAV) has shown promising therapeutic effects. [1] However, the stringent cargo limit of the vector (4,700 - 5,000 bps) [2] allows its application to only a fraction of the patients with mutations in relatively small pathogenic genes. For example, according to our recent genetic survey of Japanese patients with retinitis pigmentosa, the most frequent inherited retinal degeneration, more than 90% were shown to have mutations in larger genes untreatable by AAV-mediated gene supplementation. [3] Thus, vast majority of these patients require other approaches other than AAV-mediated gene supplementation to treat their mutations, except for rare exceptions.[4] Recently, the CRISPR-Cas9-mediated allele knock-out genome editing strategy, based on non-homologous end joining (NHEJ) has been successfully applied to correct gain-of-function mutations via AAV.[5, 6, 7, 8] One of the unique advantages of the genome editing approach is that it allows local treatment of the genome, such that the approach does not depend on the size of the target gene. However, genome editing for loss-of-function mutations in larger genes that require local replacement of the mutated sequence with a wildtype counterpart (mutation replacement) has not been successful in

55 treatment of neuronal disorders primarily affecting neurons, due to its low editing efficiency. [9,
56 10, 11, 12] This could be partly attributed to the requirement of two separate vectors for this
57 approach, in which various components including Cas9, two guide RNAs (gRNAs) and U6
58 promoters, and DNA template and flanking homology arms all needs to be contained.
59 Recently, extremely small homology arms of ~20 bps (microhomology arms), relative to the
60 conventional homology arms sized a few hundred bps or more, have been successfully
61 applied to edit mammalian genome *in vivo*. [13] This system termed microhomology-mediated
62 end joining (MMEJ) reportedly allows precise integration of a DNA donor in a desired
63 genomic location. [14] In this study, we aim to develop a single AAV vector platform for
64 mutation replacement genome editing using MMEJ. Through application of the platform in
65 mouse models of retinal dystrophy, we show that a robust restoration of the visual function
66 can be achieved, supported by an improved genome editing efficacy.
67
68 **Results**
69 First, we generated mutants of preexisting retina-specific promoters and conducted
70 *in vivo* AAV reporter assays (Fig. S1a-e and Table S1). The smallest promoter that
71 maintained neural retina-specific transcription was a 93-bp mutant *GRK1* promoter with
72 reporter expression in 65.5% of the photoreceptors, including the cones (Fig. S1c). This was

used to drive SaCas9 (3.2 Kb) expression. We tested our single-AAV vector platform in *Gnat1*$^{IRD2/IRD2}$/*Pde6c*$^{cpfl1/cpfl1}$ mice; the *Gnat1* and *Pde6c* defects in these mice cause blindness due to a functional lack of rods and cones,[15] leaving behind only a residual cortical light response to brightest flashes[16] mediated by *Gnat2*.[17] This allows the clear observation of therapeutic effects. We used our platform to correct *IRD2* mutations in *Gnat1*; these mutations constitute a homozygous 59-bp deletion in intron 4 (Fig. S2a), preventing protein expression in the rods[18], which comprise ~75% of murine retinal cells.[19] Six gRNAs designed to flank the mutation were assessed with a T7 endonuclease 1 (T7E1) assay (Fig. S2b,c and Table S2). The gRNA pair (1+4) that excised the mutation most efficiently was selected.

The constructed prototype single-AAV vector (MMEJ vector; Fig 1a and Fig. S3a,f,g) that allows mutation replacement via MMEJ was then injected sub-retinally in 6M-old blind mice. Mutations of up to a few bp were designed in the gRNA target sites flanking the donor sequence to prevent repeated cleavage of the sites after successful mutation replacement. At this age, the rods show little sign of degeneration.[20] Six weeks later, histology showed scattered GNAT1-positive photoreceptors, indicating successful genome editing (Fig. 1b). Injection of a modified MMEJ vector that tagged SaCas9 expression with a fluorescent reporter (Fig. S3b) showed GNAT1 immunoreactivity

exclusively in the cells and retinal area with reporter expression (Fig. 1c), suggesting a causal relationship between SaCas9 and GNAT1 expression. Furthermore, histology showed no sign of accelerated cone degeneration as a side effect of the treatment, although we have no evidence that genome editing occurs in cones (Fig. 1d and S1c). Next, we investigated the effects of *Gnat1* mutation replacement on mRNA expression of related genes (Fig. 1e). The expression of *Rho* and *Pde6b*, both of which cooperate with *Gnat1* to signal phototransduction in rods,[21] and of *Rcvrn*, a marker of both rods and cones, were not reduced in the eyes of untreated blind mice and remained unchanged after the treatment. However, the expression of the rod bipolar cell marker *Pkcα*, which had been reduced to 29.3% of its expression in the controls, nearly doubled to 50.0% following the treatment, indicating that the treated rods interacted with the downstream bipolar cells. Meanwhile, the absolute editing efficiency deduced from *Gnat1* mRNA expression was ~12.7% (Fig. 1f). In contrast, when microhomology arms (MHAs) or gRNA target sites flanking the donor sequence were removed from the prototype MMEJ vector (Fig. S3c,d), the efficiency was dramatically reduced, consistent with mutation replacement mediated by MMEJ. Furthermore, testing with a 6-Hz flicker electroretinogram (ERG), which reflects the number of functional photoreceptors, revealed responses averaging 11.2% of that in the control mice (Fig. 1g). The effect was severely diminished after the intravitreal injection of LAP4, a

glutamate analog that blocks synaptic transmission between the photoreceptors and ON-bipolar cells.[20] This is consistent with functional connection of the treated rods with downstream neural circuits. The result was further corroborated by a single-flash ERG paradigm: mice pretreated with MMEJ vector and then injected with LAP4 showed reduced b-waves generated by the ON bipolar cells including the rod bipolar cells, and preserved a-waves driven by rods (Fig. 1h). Again, the modified vectors without MHAs or gRNA target sites, showed no discernable response in either ERG protocol, supporting the specific role of MMEJ in mutation replacement. These results were consistent with ~10% success in mutation replacement via MMEJ in the rods and functional integration of the treated cells into the retinal circuitry.

Next, we carried out PCR-based sequencing analyses of the on-target site *in vitro* (Fig. S4) and *in vivo* (Fig. 2). The *in vitro* analysis showed a 10.3% success rate after MMEJ mutation replacement, higher than the rate of 3.8% with a different mutation replacement strategy (homology-independent targeted integration, HITI; Fig. S3e-g and S4a,b).[9] Similarly, the success rate of *in vivo* mutation replacement in the genome-edited rods was 11.1% and 4.5% for the MMEJ and HITI approaches, respectively, at 1M post-treatment (Fig. 2a). Gross estimate of absolute successful editing rate in the rods, uncorrected and partially corrected also for the sensitivity of the sequence analysis, was 4.7% and 9.1% for the MMEJ

approach (Fig. 2b-d). In both the *in vitro* and *in vivo* analyses, MMEJ vectors without MHAs or gRNA target sites did not result in any successful mutation replacements. Meanwhile, the major editing outcome was deletion caused by a simple excision of the *IRD2* mutation for both *in vitro* and *in vivo* analyses. Unplanned *in vivo* on-target integrations of the AAV genome were present, but at a lower rate than deletions. Extended *in vivo* on-target site sequencing and mRNA analysis (Fig. 2a-f) conducted 3M post-treatment revealed a similar absolute success rate (corrected editing rate of 11.0%) accompanied by the sustained or slightly reduced expression of SaCas9 mRNA and gRNAs (Fig. 2g,h), demonstrating the stability of the platform. The result also indicates that the treatment effect nearly plateaus by 1M. Although accurate estimation by PCR based sequencing is difficult, the results support the stable ~10% absolute editing efficiency at the genome level in the rods with MMEJ-mediated mutation replacement.

Then, off-target analysis was performed with a T7E1 assay and PCR-based sequencing of 14 predicted sites (7 for each gRNA, Table S2). These showed no mutation events in retinas collected 1M after MMEJ vector injection (Fig. S5). In these sites, whole genome sequencing of 4 retinas of 4 mice collected 1M post-injection (average read depth of 158 per base) and an additional 3 retinas of 3 mice collected 4M post-injection (average read depth of 126 per base) revealed no off-target events (Table S3). In addition, we listed

up additional 59 potential off-target sites in an unbiased manner, by selecting all variants in whole genome sequence data that were present in 3 independent samples collected after the therapeutic transfection of murine Neuro2A cells, but were not present in a single sample collected before transfection (Table. S3). No indels were observed in these sites using the whole genome sequence data from the 7 retinas also used for the on-target analysis (average read depth of 219 per site). Furthermore, there was no evidence of AAV integration into the mouse genome outside of the on-target site. Together, these results indicate that off-target indel formation was rare, if it occurred at all.

Next, we investigated the therapeutic effects of MMEJ-mediated mutation replacement. Light sensitivity in the visual cortex was assessed with flash visually evoked potentials (fVEPs). Surprisingly, cortical responses contralateral to the treated eye revealed a ~10,000-fold (range: 1,000 – 100,000-fold) improvement in light sensitivity, equivalent to gene supplementation in ~70% of the photoreceptors (Fig. 3a, S1f, S3h, and S6a) with greater ERG rescue (Fig. S6b,c).[16] Changes in light-induced behavior (fear conditioning, Fig. 3b) also reflected this improvement. Furthermore, cortical responses to phase-reversal gratings of various spatial resolutions, i.e., the pattern VEP (pVEP), showed larger amplitudes post-treatment (Fig. 3c). The threshold of spatial resolution of vision (i.e., visual acuity), determined by measuring the optokinetic response (OKR), was restored in the

163 treated mice to 59.1% of the control mice, also similar to the effect of gene supplementation
164 (Fig. 3d). Taken together, MMEJ-mediated *Gnat1* mutation replacement allowed substantial
165 improvement of light sensitivity and visual acuity, comparable to the effects delivered by
166 gene supplementation.

167 We also used MMEJ-mediated mutation replacement to treat 2M-old *Gnat1*$^{IRD2/IRD2}$
168 mice, which retain cone function and serve as a model of human retinal dystrophy.[22] In the
169 early course of the disease, patients suffer from severe loss of light sensitivity with
170 preserved visual acuity. [22] A histological analysis showed scattered GNAT1-postive
171 photoreceptors in the treated mice (Fig. 4a). RT-PCR measurement indicated that absolute
172 genome editing efficiency was 7.2% (Fig. S7a). The fVEP analysis showed a ~1,000-fold
173 increase in light sensitivity (Fig. 4b). This was confirmed behaviorally in a fear conditioning
174 experiment (Fig. 4c). However, the improvement in retinal function could not be isolated
175 from preexisting cone function by ERG testing, and visual acuity remained unchanged in
176 pVEP and OKR testing (Fig. S7b-d). These results show that the therapeutic effects of our
177 platform extended to an animal model of human disease.
178
179 **Discussion**

This study shows that mutation replacement genome editing with a single AAV vector can achieve striking improvements in light sensitivity and visual acuity comparable to that of gene supplementation.[16] The results showed that the gene supplementation can treat by far a larger number of retinal neurons compared to the mutation replacement genome editing, resulting in substantially larger ERG responses directly proportional to the increased number of light-responsive photoreceptors in the former. However, the light sensitivity as defined by dimmest recognizable light stimulus and visual acuity was not very different between the two treatment approaches (Figure 3a right lower panel). This is because thresholds of these visual perceptions reflect functional integrity of defined number of photoreceptors rather the total number of treated retinal neurons.

This therapeutic platform renders a major step forward from the dual vector-based mutation replacements, which generally yield an absolute editing efficiency of less than ~5%[10, 11, 12] in post-mitotic cells, including 4.5% efficiency at the level of mRNA in the retinal pigment epithelium in a rat model of retinal dystrophy, [9] compared to the efficiency of up to ~10% shown here by genomic, mRNA, and functional analysis. This paves the way for treating loss-of-function mutations in larger genes, for which conventional gene supplementation therapy or NHEJ-based genome editing strategies are not generally feasible.

198

199 **Methods**

200

201 **Animals**

202 *Pde6c*$^{cpfl1/cpfl1}$*Gnat1*$^{IRD2/IRD2}$ mice (i.e., blind mice) were derived from *Gnat1*$^{IRD2/IRD2}$

203 mice (Takeda, Japan),[18] which are rod-defective, and *Pde6c* $^{cpfl1/cpfl1}$ mice (Jackson

204 Laboratory, Bar Harbor, ME),[23] which are cone-defective. The phenotype of these mice has

205 been previously studied and reported.[16] For the *in vivo* reporter assay, an AAV vector (1 ×

206 10^{12} gc mL^{-1}) was injected (1.5 μ L per injection) into the ventral subretinal space of

207 3-month-old C57BL/6J mice (Japan SLC Inc., Hamamatsu, Japan) as previously reported.

208 [24] For mutation placement genome editing, the AAV vector (1 × 10^{12} gc mL^{-1}) was injected

209 (1.5 μ L per injection) into the dorsal and ventral subretinal space of

210 *Pde6c*$^{cpfl1/cpfl1}$*Gnat1*$^{IRD2/IRD2}$ mice (6-month-old) and *Gnat1*$^{IRD2/IRD2}$ mice (2-month-old).

211 Control animals comprised age-matched *Pde6c* $^{cpfl1/cpfl1}$ mice or C57BL/6J mice (Japan SLC

212 Inc., Hamamatsu, Japan). The surgical procedures were performed after intraperitoneal

213 administration of a mixture of ketamine (37.5 mg kg^{-1}) and medetomidine (0.63 mg kg^{-1}). The

214 medetomidine was reversed by intraperitoneal administration of atipamezole (1.25 mg kg^{-1})

215 after the surgery. Sample sizes were calculated using an on-line sample size calculator

(https://www.stat.ubc.ca/) adopting a two-sided alpha-level of 0.05, 80% power. The parameters included the means and standard deviation predicted from a previous study we conducted with a similar experimental approach to evaluate effects of AAV-mediated gene supplementation therapy on a group of mice that had a similar genetic background.[16] Rarely, the sample size was limited by the availability of mice. The mice were handled in accordance with the ARVO Statement On the Use of Animals in Ophthalmic and Vision Research and the Tohoku University guidelines for the care and use of animals. All experimental procedures were conducted after approval by the relevant committee for animal experiments at Tohoku University Graduate School of Medicine.

Miniaturization of photoreceptor-specific promoter

Various known small promoters (Table S1) were tested before deletion mutant promoters were synthesized by modifying the *RCV* promoter [25] or *GRK1* promoter [26] (Figure S1c, Thermo Fisher Scientific, Waltham, MA; Eurofins Genomics, Tokyo, Japan). They were each sub-cloned into a pAAV-MCS Promoterless Expression Vector (Cell Biolabs Inc., San Diego, CA) containing an enhanced green fluorescent protein (EGFP) gene as a reporter, as previously described. [24, 27] AAV2/8 containing the reporter constructs were generated and purified following the method described below. Each virus was injected into 2 eyes of

C57BL/6J mice. The eyes were collected 1 week after the injection and were processed for histological assessment as described below.

Selection of gRNAs

Three gRNAs each were designed using Cas-Designer (http://www.rgenome.net/cas-designer/) on both sides of the mutation in the intron 4 and exon 4 of *Gnat1,* as displayed in Figure S2 (Assembly: GRCm38/mm10). Oligos for each gRNA were subcloned with pX601 vector (gRNA expression plasmid, addgene #61591). Neuro2a cells (Cell Resource Center for Biomedical Research, Tohoku University, Sendai, Japan) were transfected with an gRNA expression plasmid using lipofectamine 3000 transfection reagent (Thermo Fisher Scientific). Genomic DNA was extracted 72 hrs post-transfection using a DNA extraction kit (QIAamp DNA Mini kit; Qiagen, Hilden, Germany). This was subjected to a T7E1 assay following the manufacturer's instructions (New England Biolabs, Ipswich, MA). In brief, genomic fragments containing the gRNA target site were amplified with PCR and purified using NucleoSpin Gel and a PCR Clean-up kit (Macherey-Nagel, Düren, Germany). Then 200 ng of each of the PCR products derived from the transfected and non-transfected cells were denatured at 95º C for 5 min and reannealed, then digested with T7E1 for 30 min at 37º C, followed by electrophoresis in 2%

agarose gel. After measuring the density of the bands with ImageJ, %indels was calculated following the formula: 100 × (1−(1−cleaved band intensity/total band intensities)1/2). [28] The sequences of all the PCR primers used in this study are presented in Table S2.

Construction and purification of plasmid and AAV vectors

The all-in-one CRISPR/SaCas9 plasmid (pX601) for mutation replacement genome editing was assembled as shown in Fig. S1. The 93-bp *GRK1* promoter (*GRK1-93*) was used to drive SaCas9 (Ac. No. CCK74173.1; from pX601) expression. Oligonucleotides for the donor template, which comprised the flanking micro-homology arms, gRNA target sites and the donor sequence, were synthesized and inserted into the vector using a DNA ligation kit (Clontech, Mountain View, CA). To avoid repeated cleavage after successful mutation replacement, mutations were introduced in the flanking gRNA target sites. The 4 bp mutation in the 5' gRNA-1 target site inside exon 4 was selected using codon optimization tool GENEisu (http://www.geneius.de/GENEius/). For selecting 1 bp mutation in the 3' gRNA-4 target site, the corresponding genomic sequences from *Mus musculus*, *Mus Caloli*, *Mus phari* and *Rattus norvegicus* were aligned by ClustalW (https://clustalw.ddbj.nig.ac.jp/). The sequences were perfectly conserved except for a single variant in *Rattus norvegicus*, which was chosen for inducing mutation. Mutations at

both target sites were confirmed with off-target site analysis tool CRISPOR (http://crispor.tefor.net/) to yield lowest probability of cleavage (Cutting frequency determination score of 0.00). For labeling of SaCas9 expression, 2A peptide and mKO1 (monomeric Kusabira-Orange 1) red fluorescence protein cDNA (MBL, Nagoya, Japan) were inserted downstream of SaCas9 into the vector using a NEBuilder HiFi assembly kit (New England Biolabs). For construction of plasmid used for cell sorting, MMEJ vector was modified so that 2A peptide and EGFP cDNA (Clontech) were inserted downstream of the *SaCas9* driven by *CMV* promoter replaced for the *GRK1-93* promotor. The NoMHA (no mirohomology arm), NoTS (no target site) and HITI (homology-independent targeted integration) plasmids was assembled as shown in Fig. S1. Each fragment was synthesized and inserted into the vector using the same regents described above. We also constructed a plasmid vector for gene supplementation of *GNAT1* as previously described [16] (shown in Fig.S1h). In brief, full length *GNAT1* cDNA (KIEE3139; Promega Corp., Madison, WI) was subcloned downstream of the ubiquitous *CMV* promoter into the AAV-MCS vector (Cell Biolabs Inc).

Then, the constructed plasmid vectors were used for *in vitro* assays or assembled into AAV2/8. In brief, each vector was co-transfected with AAV2rep/AAV8cap vector (pdp8; Plasmid Factory, Bielefeld, Germany) in HEK293T cells (Thermo Fisher Scientific) using PEI

288 (Polysciences Inc, Warrington, PA). AAV particles was extracted in PBS and purified with an
289 AKTA prime plus chromatography system (GE Healthcare, Chicago, IL) on an AVB
290 Separose HP column (GE Healthcare), as previously described. [24, 27]
291
292 **RT-PCR**
293 RT-PCR was carried out as described previously.[27] Total RNA was purified from the
294 mouse retinas using the miRNeasy plus mini kit (Qiagen) and reverse-transcribed with
295 SuperScript III (Thermo Fisher Scientific). qRT-PCR was performed with an initial
296 denaturation step at 95° C for 20 s, followed by 40 cycles at 95° C for 3 s and 60° C for 20 s
297 (7500 Fast Real-Time PCR System; Thermo Fisher Scientific). Taqman probes for *Gnat1*
298 (Mm01229120; Thermo Fisher Scientific), *Gapdh* (Mm99999915; Thermo Fisher Scientific),
299 *Pde6b* (Mm00476679; Thermo Fisher Scientific), *Pkca* (Mm00440858; Thermo Fisher
300 Scientific), *Rho* (Mm01184405; Thermo Fisher Scientific), *Rcvrn* (Mm00501325; Thermo
301 Fisher Scientific) and *SaCas9* (AP2XCCY; Thermo Fisher Scientific) were used. For
302 SaCas9 and gRNA scaffold, primers and probes were designed and used as previously
303 described. [4] Each mRNA expression was determined by plotting CT values on the standard
304 curve generated by serially diluting the control sample (C57BL/6J mice retinal cDNA or AAV
305 injected retinal cDNA).

306

307 **Western blot**

308 The eyes were harvested 6 weeks (1.5M) after the AAV injection. The retina and
309 RPE/choroid complex were then collected separately and placed on ice. The tissues were
310 dissolved in RIPA buffer and the total protein concentration was measured with a Pierce
311 BCA protein assay kit (Thermo Fisher Scientific). Proteins (15 μg each) were separated
312 based on their molecular weight with SDS–PAGE on 10% Mini-PROTEAN gels (Bio-Rad,
313 Hercules, CA) and then transferred to PVDF membranes (Millipore, Billerica, MA).
314 Membranes were blocked with 5% skim milk for 1 hr, incubated with rabbit anti-GFP
315 antibody (#598, 1/2500; MBL) for 1 hr, and then incubated with horseradish peroxidase
316 (HRP)-conjugated anti-rabbit IgG antibodies (A0545, 1/2000; Sigma-Aldrich) for 1 hr. The
317 immunogenic signal was detected with ECL prime (GE Healthcare). The membrane was
318 stripped and incubated with anti-beta-actin (F5316, 1/2000; Sigma-Aldrich, St. Louis, MO),
319 incubated with HRP-conjugated anti-mouse antibodies (#31430, 1/2000; Thermo Fisher
320 Scientific), and detected with ECL prime.

321

322 **Immunohistochemistry**

323 Immunohistochemistry was performed as described previously.[27] Six weeks (1.5M)

after the AAV injection, the eyes were fixed in 4% paraformaldehyde. They were then either embedded in OCT compound and sectioned using a cryostat to generate retinal sections, or the RPE/choroid complex was separated from the retina and then flattened by creating 4 incisions from the periphery to the optic nerve, thereby resulting in a clover-shaped RPE/choroid flatmount. The retinal sections were blocked with 5% normal goat serum for 30 min, incubated with mouse anti-mKO1 monoclonal antibodies (M104-3M, 1/200; MBL), rabbit anti-M-opsin antibodies (AB5405, 1/1000; Millipore) or rabbit anti-recoverin (AB5585, 1/5000; Millipore) and Alexa Fluor 488 conjugated PNA (10 μg/mL, Thermo Fisher scientific) for 1hr, incubated with Alexa Fluo 568-conjugated anti-mouse IgG antibodies (1/500; Thermo Fisher Scientific) or Alexa Fluo 568-conjugated anti-rabbit IgG antibodies (1/500; Thermo Fisher Scientific) for for 1hr, and DAPI (Vector Labs, Burlingame CA) for additional 45 min. For the reporter assay, RPE/choroid flat mounts were stained with only DAPI for 45 min before imaging. For the analysis of GNAT1 expression, immunohistochemistry was carried out using a TSA Plus Fluorescein System (Perkin-Elmer, Waltham, MA, USA) following the manufacturer's instructions. In brief, the sections were blocked with 1% skim milk for 1 hr, incubated with rabbit anti-GNAT1 antibodies (ab74059, 1/200; Abcam, Cambridge, UK) for 1 hr, incubated with HRP-conjugated anti-rabbit IgG antibodies (A0545, 1/2000; Sigma-Aldrich) for 1 hr, and then stained with TSA reagent and/or DAPI for an

342 additional 45 min. The retinal flat mounts were stained as previously described.[29] In brief,
343 the isolated eyes were fixed in 4% paraformaldehyde. Then they were treated with 3
344 freeze/thaw cycles. For the analysis of Gnat1 expression, the retinas were blocked with 1%
345 skim milk for 1 hr, incubated with rabbit anti-GNAT1 antibodies (ab74059, 1/200; Abcam,
346 Cambridge, UK) overnight, incubated with HRP-conjugated anti-rabbit IgG antibodies
347 (A0545, 1/2000; Sigma-Aldrich) for 1 hr, and then stained with TSA reagent (Perkin-Elmer).
348 For the analysis of mKO1 expression, the retinas were blocked with 5% normal goat serum
349 for 1 hr, incubated with mouse anti-mKO1 monoclonal antibodies (M104-3M, 1/200; MBL)
350 overnight, incubated with Alexa Fluo 568-conjugated anti-mouse IgG antibodies (1/500;
351 Thermo Fisher Scientific) for 1hr. Images were acquired on a Zeiss LSM780 confocal
352 microscope (Carl Zeiss, Jena, Germany).
353
354
355 **Electrophysiological assessment**
356 Basic equipment and techniques for ERG and fVEP recordings were carried out as
357 previously described.[30] Scotopic 6-Hz flicker ERGs were recorded following a previously
358 published protocol[31] with modifications. We used flash intensities at 7 steps, ranging from
359 -6.0 to 0 log.cd.s m^{-2}, separated by 1.0 log units. For each step, after 10 seconds of

adaptation, 400 msec sweeps were recorded 50 times and averaged.

Standard single flash ERGs were recorded following a previously published protocol. [16] In brief, we used flash intensities comprising 10 steps, ranging from -7.0 to 2.0 log.cd.s m^{-2}, separated by 1.0 log units (Fig S6c). Then, the standard protocol was optimized for an accurate estimation of the small effect of MMEJ-mediated mutation replacement in *Pde6c*$^{cpfl1/cpfl1}$*Gnat1*$^{IRD2/IRD2}$ mice, in which a fixed flash (1.0 log.cd.s m^{-2}) separated by 10 sec intervals with increased averaging of 50 times (compared to 2 times in the standard protocol for this flash intensity) were applied (Fig. 1h). For assessing synaptic transmission between photoreceptor and ON-bipolar cells, group III mGlu agonist L-AP4 (L-2-amino-4-phosphonobyturic acid, ab12002, 50 mM; Abcam) was injected into the vitreous of the mice at 3 W after treatment with MMEJ vector and ERGs were recorded before (to ensure successful mutation replacement) and 20hr after injection following the protocol described. [20]

Surgical implantation of the VEP electrodes was carried out as previously described[30, 32] 5 weeks post-injection, and recording was performed a week later. For recording fVEPs, we used flash intensities at 9 steps, ranging from -7.0 to 1.0 log.cd.s m^{-2}, separated by 1.0 log units. The light sensitivity of the visual cortex was determined by identifying the dimmest light condition that yielded an amplitude of the negative trough

(P1-N1) or a positive peak (N1-P2) over 25 µV during fVEP recording. To record pVEPs, we used black (3 cd m^{-2}) and white (159 cd m^{-2}) vertical stripes of equal width (average luminance: 81 cd m^{-2}) with different spatial resolutions (0.42, 0.35, 0.28, 0.21, 0.14, 0.07, 0.05, 0.03, 0.02 and 0.01 cycles per degree for the *Gnat1*$^{IRD2/IRD}$ mice, and 0.21, 0.14, 0.07, 0.05, 0.03, 0.02 and 0.01 cycles per degree for the *Gnat1*$^{IRD2/IRD2}$*/Pde6c*$^{cpfl1/cpfl1}$ mice), as described previously.[32] The amplitudes for the negative trough (P1-N1) and positive peak (N1-P2) were plotted vertically as a function of the log spatial resolution of the stimulus (horizontally).

Behavioral tests

Fear conditioning was performed 3 weeks after the AAV treatment, as previously described, with modifications.[20] In the training session, each mouse was placed in a shock chamber with a stainless-steel grid floor (21.5 cm width × 20.5 cm depth × 30 cm height box; Ohara Medical Industry, Tokyo, Japan), located inside a sound attenuating box, and left for 2 mins to adapt to the environment. Then, the mouse was exposed to an LED light cue (535 nm, 0.015 cd m^{-2}, 2.0 Hz, 5.0 s) controlled via a stimulus controller (FZ-LU, Ohara Medical Industry) that co-terminated with a 0.8-mA foot shock (2.0-s duration). This was repeated 5 times at pseudorandomized intervals (70 - 140s) before returning the mouse to

396 the housing cage. In the testing session, which took place 24 hours after the training session,
397 the mice were returned to the same chamber to test for visually-cued memory recall. In
398 order to change the environmental context from the training session, a white floor and
399 curved wall made of thin plastic were inserted into the chamber before the test. After placing
400 the mice in the environmentally modified chamber, the mouse was allowed to adapt to the
401 environment for 4.0 minutes before being shown the light cue, which persisted for 2.0
402 minutes. The time spent freezing, as defined by an absence of movement (< 200 pixels, >
403 2.0 s), was recorded by a built-in infrared video camera. The time spent freezing during the
404 2.0 min immediately before and after presentation of the light cue was averaged using
405 pre-installed imaging software (Ohara Medical Industry).

406 Visual acuity was measured 2 weeks after the AAV injection by observing the
407 optokinetic responses of mice to rotating sinusoidal gratings presented on monitors
408 (average luminance: 62 cd m^{-2}) surrounding the mouse (Optomotry, Cerebral Mechanics,
409 Lethbridge, Canada), as reported previously.[16] This test yields independent measures of
410 right and left eye acuity based on the unequal sensitivities to pattern rotation direction, as
411 the motion in the temporal-to-nasal direction dominates the tracking response.[33] Visual
412 acuity data used in this study represented the averages of four trials conducted on four
413 consecutive days. The results obtained by testing without using a mouse served as the

414 negative control.

415

416 ***In vitro* on-target assessment**

417 Neuro2a genomic DNA was extracted 72 hrs post-transfection using a DNA

418 extraction kit (QIAamp DNA Mini kit). PCR products were sub-cloned into T-vector (pTAC2;

419 BioDynamics, Tokyo, Japan), which was used to transform a DH5a-competent cell (Toyobo,

420 Osaka, Japan). DNA from single colonies (>50 clones) were amplified by colony direct PCR.

421 Each PCR fragment was sequenced following a standard procedure using an ABI3130

422 genetic analyzer (Thermo Fisher Scientific), as described previously.[34]

423 For preparation of DNA samples used for *in vitro* analysis by whole genome

424 sequencing, successfully transfected Neuro2a cells were used. In brief, Neuro2a cells were

425 transfected with an SaCas9-2A-EGFP expression plasmid described above using

426 lipofectamine 3000 transfection reagent (Thermo Fisher Scientific). After 72hrs,

427 EGFP-positive cells were selected using FASC aria II cell sorter (BD Biosciences, Franklin

428 lakes, NJ), and genomic DNA were extracted from these cells using DNA extraction kit

429 (QIAamp DNA Mini kit).

430

431

In vivo on-target and off-target assessment

The on-target site and the 14 off-target sites (listed in Fig. S3 and Table S3, assembly: GRCm38/mm10) predicted by CRISPOR (http://crispor.tefor.net/) were amplified with PCR using the primers listed in Table S2. PCR products were subjected either to a T7E1 assay or Sanger sequencing of the PCR clones. We conducted a T7E1 assay for the 14 off-target sites, as described above in detail. PCR products of the on-target site and the14 off-target sites were sub-cloned into T-vector (pTAC2; BioDynamics, Tokyo, Japan), which was used to transform a DH5a-competent cell (Toyobo, Osaka, Japan). DNA from single colonies (>50 clones for the on-target site and >50 clones each for the off-target site) were amplified by colony direct PCR. Each on-target and/or off-target PCR fragment was sequenced following a standard procedure using an ABI3130 genetic analyzer (Thermo Fisher Scientific), as described previously.[34] Classifications of the sequenced clones are as follows: Success, mutation replaced as planned; Cleavage site indel, insertion or deletion in either gRNA cleavage site without replacement of *IRD2* mutation; AAV integration, unplanned insertion of AAV genome fragment; Deletion, simple excision of the IRD2 mutation at the two gRNA cleavage sites without an insertion; Other indel, mutations that do not belong to any of the classifications above.

Whole genome sequencing and assessment of off-target sites & AAV integration

For the genomic DNAs extracted from Neuro2A and mice, we performed whole-genome sequencing using the NovaSeq 6000 (Illumina, San Diego, CA, USA) sequencer with 151 bp paired-end reads. The amount of data per sample was made to exceed at least 100G bases. The sequencing library was constructed using the TruSeq Nano DNA Library Prep Kit (Illumina) according to the manufacturer's instructions. We prepared two reference genomes, mouse reference genome (mm10) and mm10 plus AAV genome (mm10+AAV). The sequencing reads were separately aligned to mm10 and mm10+AAV using BWA-mem (ver.0.7.17). Then, PCR duplicate reads were marked using Picard tools (ver.2.17.8). Base quality scores were recalibrated using GATK (ver.4.1.2.0) according to the GATK Best Practices (https://software.broadinstitute.org/gatk/best-practices/).

Single nucleotide variants (SNVs) and short insertions and deletions (indels) calling were performed for the WGS data to assess off-target sites. To detect variants with low variant allele frequency (VAF), we used the GATK4 Mutect2 software, which is used for somatic variant calling. The variants were called according to the GATK Best Practices. Untransfected cells and untreated mouse data were used as normal control samples data in the Mutect2 variant calling.

In addition, to investigate whether integrations of the AAV occurred in the mice genome, we identified sequencing reads that were partially mapped (soft-clipped) to the AAV genome. From those sequencing reads, we extracted the subset of reads that were also partially mapped to the mouse genome (mm10). The extracted reads were evaluated for the presence of regions in which the AAV genome was inserted into the mouse genome.

Determination of editing efficiency

Absolute editing efficiency among rods were estimated by dividing *Gnat1* expression (RT-PCR) in the treated retinas of *Pde6c*$^{cpfl1/cpfl1}$*Gnat1*$^{IRD2/IRD2}$ mice by that in the retinas of untreated *Pde6c*$^{cpfl1/cpfl1}$ mice born with wildtype copies of *Gnat*1 (N = 4). Similarly, the efficiency was estimated by dividing the 6Hz ERG response amplitudes at -1.0 log.cd.s m^{-2} in the treated eyes of *Pde6c*$^{cpfl1/cpfl1}$*Gnat1*$^{IRD2/IRD2}$ mice by those in the untreated eyes of *Pde6c*$^{cpfl1/cpfl1}$ mice (41.5 µV, average of 4 mice). When estimating the absolute efficiency by sequencing analysis of on-target site in an *in vivo* experiment, we corrected for the difference in detection efficiency (described below), arising from the difference in PCR amplicon size of the on-target site with an assumption that the difference in efficiency remains constant across various mixture of edited and unedited alleles. The proportion of rod photoreceptors among retinal cells were considered to be 0.75[19], which were also used

to calculate genome editing efficacy among rods.

To determine the difference in detection efficiency of genome edited "success" allele (670 bp amplicon) and unedited "mutant" *IRD2* allele (611 bp amplicon), 1:1 (50%) mixture (molecular ratio) of these alleles were PCR amplified, subcloned, and re-amplified by colony direct PCR in the same way as described in ***in vivo* on-target and off-target assessment**. The identity of the clones (N = 53) were determined by difference in the band size in agarose-gel electrophoresis. Against the expected sequence results of 26.5:26.5 clones, 16:37 clones were observed for success:mutant, indicating under-representation of the former by a factor of 16/26.5 = 0.60. This factor was 0.52 when competition between "Success" and even smaller "Deletion" (524 bp amplicon; the major editing outcome) was compared with a similar experiment (16:45 clones for success:deletion). In order to correct "Success" rate for unedited "mutant" *IRD2*, which comprised the major population of the clones analyzed, we carried out the same experiment to 1:19 (5%), 1:9 (10%), 1:4 (20%), and 1:1 (50%) mixture of "Success" and unedited "mutant" *IRD2* allele (molecular ratio) followed by linear regression analysis (intercept -0.154, slope 0.528). Using the results of regression analysis, we corrected only the rates of "Success" and unedited "mutant" *IRD2* allele. For example, observed absolute "Success" for MMEJ at 1 month was 0.047 (4.7%) then absolute corrected "Success" rate would be (4.7 + 0.154)/0.528 = ~9.185%. The

504 calculation yields an underestimate of genome editing, as the “Success” represent the
505 largest PCR amplicon, thus least efficiently detected, of all the other edited genomes.
506
507 **Statistical analysis**
508 Differences between pairs of groups were assessed with the paired Student’s t-test
509 (two-sided) for paired data and unpaired Student’s t-test (two-sided) for other data.
510 Differences between sets of three groups were assessed with an analysis of variance
511 (ANOVA), followed by Tukey’s test as a post-hoc analysis. Linear regression analysis was
512 carried out to generate Figure 2d. All statistical analysis was performed with JMP (SAS
513 Institute, Cary, NC). All values are expressed as the mean ± SEM. $P < 0.05$ was considered
514 statistically significant.
515
516 **Data availability**
517 The source data underlying Figs 1d-h, 2b–h, 3a-d, 4b and c and Supplementary Figs 1d,f,
518 2c, 5a, 6b, c and 7a-d are provided as a Source Data file. The datasets generated during
519 and/or analyzed during the current study not listed in the Source Data file are available from
520 the corresponding author on reasonable request.
521

522

Reference

1. Kumaran N, Michaelides M, Smith AJ, Ali RR, Bainbridge JW. Retinal gene therapy. *Br Med Bull*, (2018).

2. Wu Z, Yang H, Colosi P. Effect of genome size on AAV vector packaging. *Mol Ther* **18**, 80-86 (2010).

3. Koyanagi Y*, et al.* Genetic characteristics of retinitis pigmentosa in 1204 Japanese patients. *J Med Genet*, jmedgenet-2018-105691 (2019).

4. Maeder ML*, et al.* Development of a gene-editing approach to restore vision loss in Leber congenital amaurosis type 10. *Nat Med* **25**, 229 (2019).

5. Tsai YT*, et al.* Clustered Regularly Interspaced Short Palindromic Repeats-Based Genome Surgery for the Treatment of Autosomal Dominant Retinitis Pigmentosa. *Ophthalmology* **125**, 1421-1430 (2018).

6. Yang S*, et al.* CRISPR/Cas9-mediated gene editing ameliorates neurotoxicity in

mouse model of Huntington's disease. *J Clin Invest* **127**, 2719-2724 (2017).

7. Gaj T, Ojala DS, Ekman FK, Byrne LC, Limsirichai P, Schaffer DV. In vivo genome editing improves motor function and extends survival in a mouse model of ALS. *Science advances* **3**, eaar3952 (2017).

8. Li P*, et al.* Allele-specific CRISPR-Cas9 genome editing of the single-base P23H mutation for rhodopsin-associated dominant retinitis pigmentosa. *The CRISPR Journal* **1**, 55-64 (2018).

9. Suzuki K*, et al.* In vivo genome editing via CRISPR/Cas9 mediated homology-independent targeted integration. *Nature* **540**, 144-149 (2016).

10. Yin H*, et al.* Therapeutic genome editing by combined viral and non-viral delivery of CRISPR system components in vivo. *Nat Biotechnol* **34**, 328 (2016).

11. Yin H*, et al.* Genome editing with Cas9 in adult mice corrects a disease mutation and phenotype. *Nat Biotechnol* **32**, 551 (2014).

12. Yang Y, *et al.* A dual AAV system enables the Cas9-mediated correction of a metabolic liver disease in newborn mice. *Nat Biotechnol* **34**, 334 (2016).

13. Yao X, *et al.* CRISPR/Cas9–Mediated precise targeted integration in vivo using a double cut donor with short homology arms. *EBioMedicine* **20**, 19-26 (2017).

14. Nakade S, *et al.* Microhomology-mediated end-joining-dependent integration of donor DNA in cells and animals using TALENs and CRISPR/Cas9. *Nature communications* **5**, 5560 (2014).

15. Lamb TD. Evolution of phototransduction, vertebrate photoreceptors and retina. *Prog Retin Eye Res* **36**, 52-119 (2013).

16. Nishiguchi KM, *et al.* Retained Plasticity and Substantial Recovery of Rod-Mediated Visual Acuity at the Visual Cortex in Blind Adult Mice with Retinal Dystrophy. *Mol Ther* **26**, 2397-2406 (2018).

577 17. Allen AE, Cameron MA, Brown TM, Vugler AA, Lucas RJ. Visual responses in mice
578 lacking critical components of all known retinal phototransduction cascades. *PLoS*
579 *One* **5**, e15063 (2010).
580
581 18. Miyamoto M, Aoki M, Hirai K, Sugimoto S, Kawasaki K, Imai R. A nonsense mutation
582 in Gnat1, encoding the alpha subunit of rod transducin, in spontaneous mouse
583 models of retinal dysfunction. *Exp Eye Res* **90**, 63-69 (2010).
584
585 19. Jeon C-J, Strettoi E, Masland RH. The major cell populations of the mouse retina. *J*
586 *Neurosci* **18**, 8936-8946 (1998).
587
588 20. Nishiguchi KM*, et al.* Gene therapy restores vision in rd1 mice after removal of a
589 confounding mutation in Gpr179. *Nature communications* **6**, 6006 (2015).
590
591 21. Fu Y, Yau K-W. Phototransduction in mouse rods and cones. *Pflügers*
592 *Archiv-European Journal of Physiology* **454**, 805-819 (2007).
593
594 22. Carrigan M, Duignan E, Humphries P, Palfi A, Kenna PF, Farrar GJ. A novel

595 homozygous truncating GNAT1 mutation implicated in retinal degeneration. *Br J*
596 *Ophthalmol* **100**, 495-500 (2016).
597
598 23. Chang B*, et al.* A homologous genetic basis of the murine cpfl1 mutant and human
599 achromatopsia linked to mutations in the PDE6C gene. *Proc Natl Acad Sci U S A*
600 **106**, 19581-19586 (2009).
601
602 24. Fujita K*, et al.* In vivo cellular imaging of various stress/response pathways using
603 AAV following axonal injury in mice. *Sci Rep* **5**, 18141 (2015).
604
605 25. Wiechmann AF, Howard EW. Functional analysis of the human recoverin gene
606 promoter. *Curr Eye Res* **26**, 25-32 (2003).
607
608 26. Khani SC*, et al.* AAV-mediated expression targeting of rod and cone photoreceptors
609 with a human rhodopsin kinase promoter. *Invest Ophthalmol Vis Sci* **48**, 3954-3961
610 (2007).
611
612 27. Fujita K, Nishiguchi KM, Shiga Y, Nakazawa T. Spatially and Temporally Regulated

NRF2 Gene Therapy Using Mcp-1 Promoter in Retinal Ganglion Cell Injury. *Mol Ther Methods Clin Dev* **5**, 130-141 (2017).

28. Ran FA, Hsu PD, Wright J, Agarwala V, Scott DA, Zhang F. Genome engineering using the CRISPR-Cas9 system. *Nat Protoc* **8**, 2281 (2013).

29. Nishiguchi KM, Kaneko H, Nakamura M, Kachi S, Terasaki H. Identification of photoreceptor precursors in the pars plana during ocular development and after retinal injury. *Invest Ophthalmol Vis Sci* **49**, 422-428 (2008).

30. Tomiyama Y*, et al.* Measurement of Electroretinograms and Visually Evoked Potentials in Awake Moving Mice. *PLoS One* **11**, e0156927 (2016).

31. Michalakis S*, et al.* Restoration of cone vision in the CNGA3−/− mouse model of congenital complete lack of cone photoreceptor function. *Mol Ther* **18**, 2057-2063 (2010).

32. Tokashiki N, Nishiguchi KM, Fujita K, Sato K, Nakagawa Y, Nakazawa T. Reliable

631 detection of low visual acuity in mice with pattern visually evoked potentials. *Sci Rep*
632 **8**, 15948 (2018).
633
634 33. Douglas RM, Alam NM, Silver BD, McGill TJ, Tschetter WW, Prusky GT.
635 Independent visual threshold measurements in the two eyes of freely moving rats
636 and mice using a virtual-reality optokinetic system. *Vis Neurosci* **22**, 677-684 (2005).
637
638 34. Nishiguchi KM*, et al.* Whole genome sequencing in patients with retinitis pigmentosa
639 reveals pathogenic DNA structural changes and NEK2 as a new disease gene.
640 *Proceedings of the National Academy of Sciences* **110**, 16139-16144 (2013).
641

642 **Acknowledgements**

643 We thank Ms Misane Uchiike for her help with the experiments and Professor Carlo Rivolta
644 for the critical comments on the manuscript. This work was supported in part by the Japan
645 Agency for Medical Research and Development (KMN, 18ek0109213h0002). The
646 manuscript was edited by a professional English editing service (Mr. Tim Hilts). We thank
647 the Biomedical Research Core of Tohoku University Graduate School of Medicine for
648 technical support.

649

650 **Author contributions**

651 KMN conceived and designed the experiments. KMN and KF performed the experiments

652 and analyzed the data. FM carried out *in slico* analysis. SK helped in vitro experiments.

653 KMN wrote the manuscript and KMN and TN obtained the funding.

654

655 **Competing financial interests**

656 KMN, KF, and TN are listed as inventors in a patent application related to this work. The

657 Departments of Advanced Ophthalmic Medicine and Ophthalmic Imaging and Information

658 Analytics are endowed departments, supported by an unrestricted grant from Senju

659 Pharmaceutical Co. (Osaka, Japan) and Topcon Co. Ltd. (Tokyo, Japan), respectively.

660 These funders had no role in the study design, data collection and analysis, decision to

661 publish, or preparation of the manuscript.

662

663

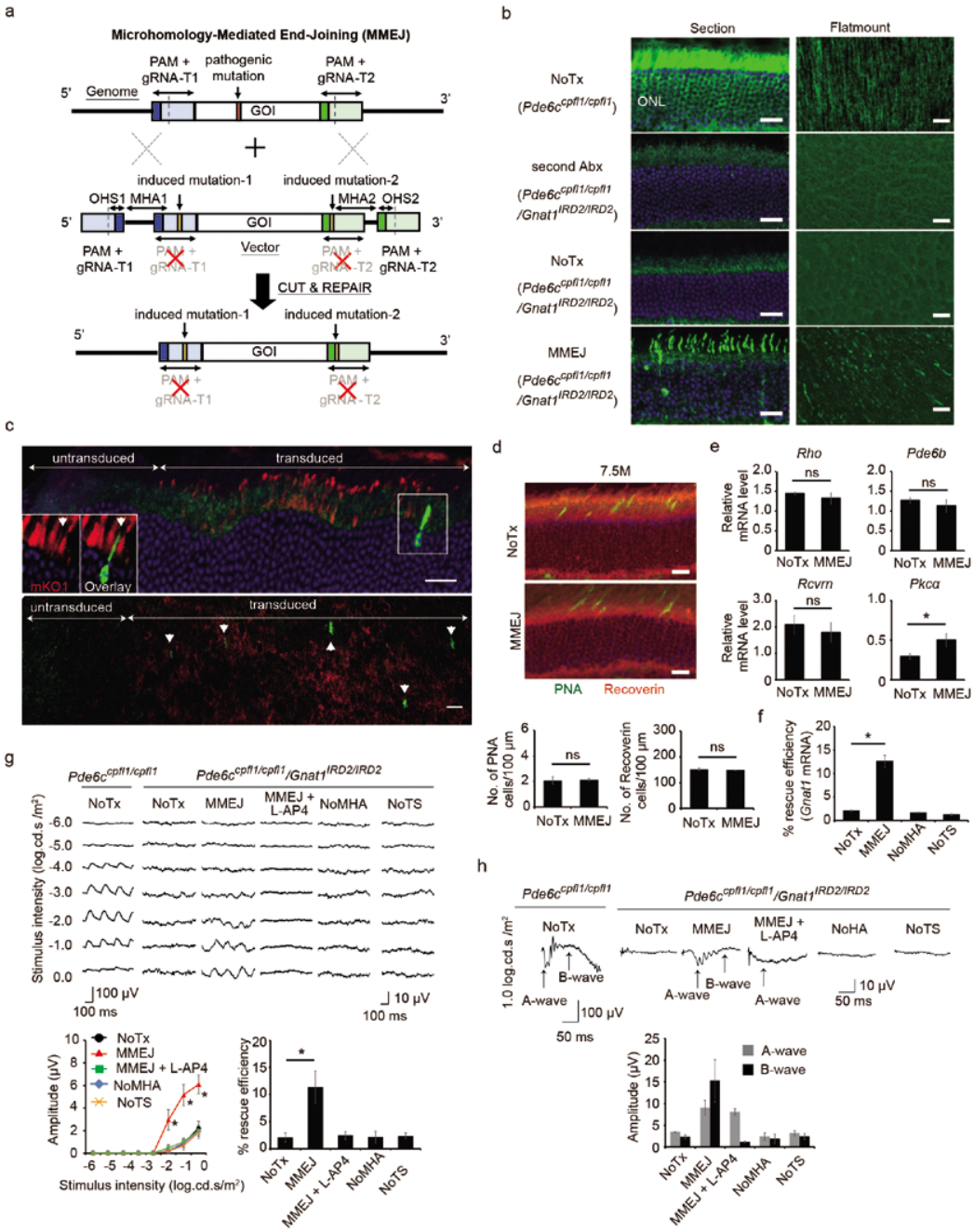

Fig 1. *In vivo* characterization of mutation replacement genome editing in *Pde6c*$^{cpfl1/cpfl1}$*Gnat1*$^{IRD2/IRD2}$ mice

a. Illustration of MMEJ-mediated mutation replacement. Genome of interest (GOI) with and without the mutation are excised at the flanking gRNA target sites (gRNA-T1 and -T2; dotted line) from mouse genome and AAV vector, respectively, by SaCas9 and two gRNAs. GOI without mutation is inserted into the genome using micro homology arms (MHA), thereby correcting the mutation. **b.** GNAT1 staining. GNAT1-positive photoreceptors (arrowhead) were observed (section, left; flatmount, right). **c.** Co-localization of Kusabira Orange (mKO1) probing SaCas9 expression and GNAT immunopositivity (inset). Scattered GNAT-positive cells were observed only in the area transduced with mKO1 (section, top; flatmount, bottom). Note, oversized reporter vector (5,201 bp) drastically reduced editing efficiency. N = 4 **d.** PNA and recoverin staining with quantification. **e.** RT-PCR of *Rho*, *Pde6b*, *Rcvrn*, and *Pkcα* (relative to *Pde6c*$^{cpfl1/cpfl1}$ mice; N = 4 for all). **f**. Rescue efficiency by RT-PCR of *Gnat1* (relative to *Pde6c*$^{cpfl1/cpfl1}$ mice; N = 4 for all). **g.** 6-Hz flicker ERGs. N = 9, 9, 4, 4, and 4 for No treatment (NoTx), MMEJ, MMEJ+L-AP4, NoMHA, NoTS, respectively. In MMEJ+L-AP4, MMEJ vector and L-AP4 were sequentially injected. Amplitudes (1.0 log.cd.s./m^2) relative to those of *Pde6c*$^{cpfl1/cpfl1}$ mice indicate %rescue efficiency (bottom right). **h.** Single flash ERGs. The same group of mice used in **g**. Scale bar: 20 µm; Data represent mean ± S.E.M.; *P < 0.05; ns, not significant; PAM, protospacer

686 **b.** adjacent motif, OHS, over-hanging sequence; Abx, antibodies; NoTS, no gRNA target

687 sites.

688

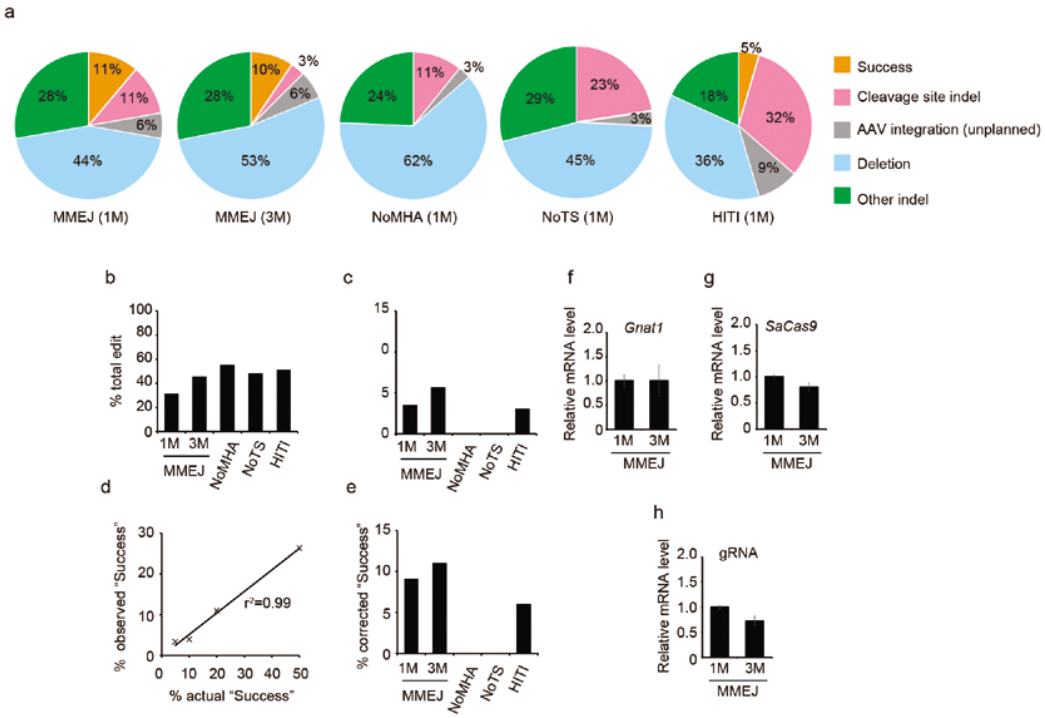

689

690 **Fig 2. *In vivo* assessment of the on-target site following mutation replacement**

691 **therapy in *Pde6c*$^{cpfl1/cpfl1}$*Gnat1*$^{IRD2/IRD2}$ mice**

692 **a.** Breakup of sequencing results of the on-target site in the genome edited clones amplified

693 from the retina collected 1M or 3M post-injection. MMEJ, NoMHA, and NoTS represents

694 injection of protype MMEJ vector, MMEJ vector without microhomology arms, and MMEJ

695 vector without gRNA target sites, respectively. HITI represents homology-independent

696 targeted integration strategy. See Fig. S3 for vector map. Total clones sequenced were 57,

70, 67, 64 and 86 for MMEJ (1M), MMEJ (3M), NoMHA (1M), NoTS (1M), and HITI (1M), respectively. “Success” indicates successful mutation replacement. “Cleavage site indel” represents indels in either gRNA cleavage site without replacement of *IRD2* mutation (see Online Methods for detail). Note, co-existing mutation replacement and cleavage site indels, which is expected to occur as a consequence of repeated cleavage at the gRNA site was not observed. **b.** Total editing rate. Percentage of clones that showed any sign of genome editing among the total clones analyzed, which were obtained by subcloning PCR amplicons of the retinal genome of the treated eyes (using primer pairs shown in Figure S4a and Table S2). **c.** Absolute success rate in the rods, assuming the cells comprise 75% of retinal neurons. **d.** Estimation of detection efficiency of “Success” allele by subcloning and PCR. Observed % “Success” (vertical axis) were obtained by distinguishing the identity of the clones derived from PCR products amplified from mixture of “Success” and “Deletion” DNA templates at various ratio (horizontal axis). Total clones sequenced in this experiment were 61, 52, 64 and 61 for 5%, 10%, 20%, and 50% mixtures (rate of “Success” DNA versus total DNA), respectively. Intercept = -0.154, slope = 0.528, r^2 = 0.99. **e**. Estimated absolute success rate in the rods corrected for by the detection efficiency of “Success” alleles relative to “Deletion allele” that comprised the major sequencing outcome in **a**, assuming 75% of retinal neurons are the rods. **f**. RT-PCR of *Gnat1* at 1M (N = 4) and 3M (N = 3). **g**. RT-PCR

715 of *SaCas9* at 1M (N = 4) and 3M (N = 3) post-injection. **h**. RT-PCR of gRNA at 1M (N = 4)

716 and 3M (N = 3) post-injection. Data represent the mean ± S.E.M.; *$P < 0.05$.

717

718

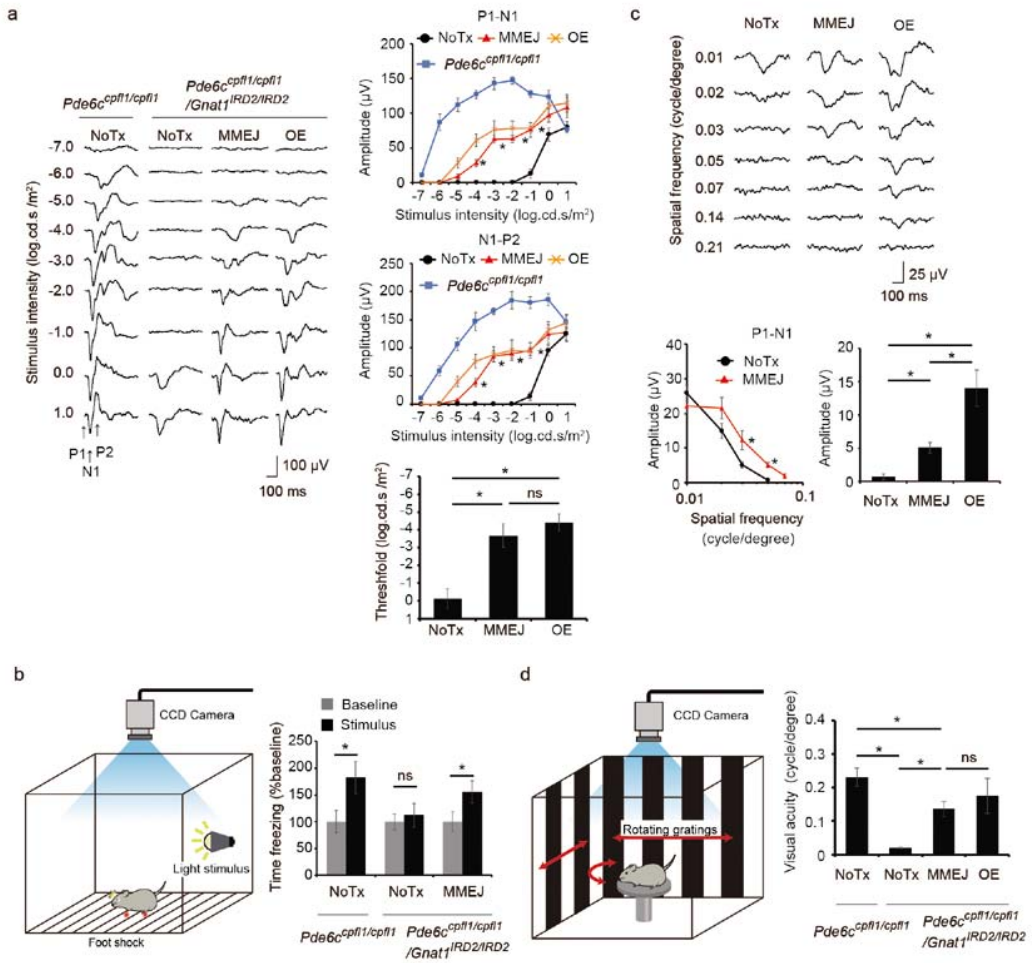

719

720 **Fig 3. Visual restoration by *in vivo* mutation-replacement genome editing in**

721 ***Pde6c*$^{cpfl1/cpfl1}$*Gnat1*$^{IRD2/IRD2}$ mice**

a. Flash visually evoked potentials (fVEP) of the visual cortex contralateral to the eyes in response to flashes of various intensities. MMEJ indicates eyes treated with *Gnat1* mutation replacement (N = 9) and OE (over-expression) indicates those with *Gnat1* gene supplementation (N = 6), both delivered by single AAV. NoTx refers to untreated eyes (N = 9). Control *Pde6c*$^{cpfl1/cpfl1}$ mice (N = 5). Note, light sensitivity as defined in the Methods was increased by ~4 log unit after MMEJ-mediated genome editing, which was not significantly different to the effect mediated by OE (right lower panel). **b.** Pattern VEPs. N = 11, and 10 for MMEJ and untreated, respectively. **c.** Fear conditioning test. Freezing time before (Baseline) and during (Stimulus) presentation of fear-conditioned light cue from MMEJ treated (N = 9) and untreated (N = 6) mice. **i.** pVEPs from MMEJ treated (N = 9) and untreated (N = 5) mice. **d.** Optokinetic response. Note threshold of spatial resolution of vision (visual acuity) was not different in the MMEJ and OE. N = 10, 7, and 4 for MMEJ, OE, and NoTx, respectively. Control *Pde6c*$^{cpfl1/cpfl1}$ mice (N = 6). Data represent the mean ± S.E.M.; *P < 0.05; nd, non-detectable; ns, not significant.

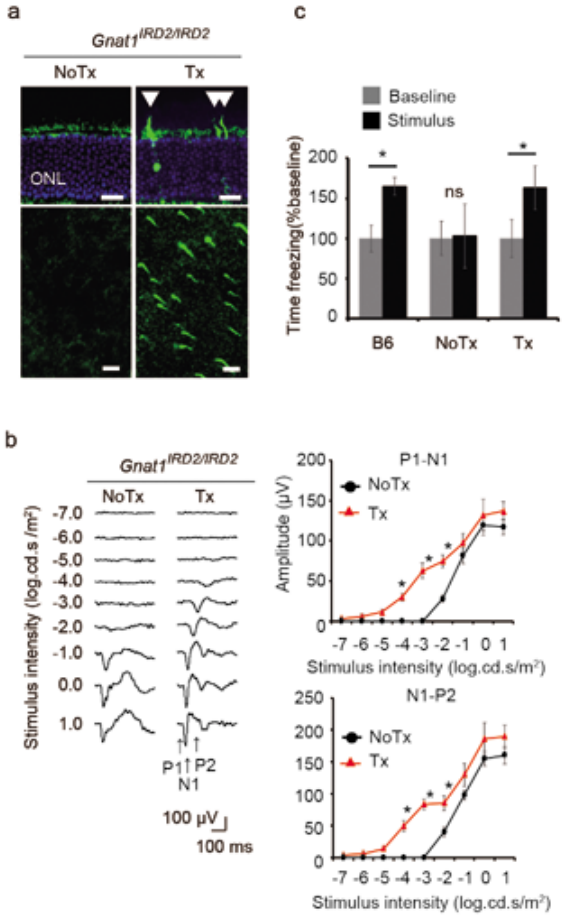

Fig 4. *In vivo* mutation replacement genome editing in a mouse model of retinal degeneration

a. GNAT1-positive photoreceptors (arrowhead) following treatment of *Gnat1*$^{IRD2/IRD2}$ mice shown in a retinal section (top) and a flatmount (bottom). Scale bar: 20 µm. **b.** fVEPs recorded from contralateral visual cortices in treated and untreated eyes of the same mice. (N = 7). **c.** Fear conditioning test, showing freezing time before (Baseline) and during (Stimulus) presentation of fear-conditioned light cue. Treated (Tx, N = 7) and untreated

745 (NoTx, N = 6) *Gnat1*$^{IRD2/IRD2}$ mice and CL57B6 mice (B6, N = 6). Data represent the mean ±

746 S.E.M.; *P < 0.05; ONL, outer nuclear layer. ns, not significant.

747